

## ANGULAR MOMENTUM TRANSFER IN DARK MATTER HALOS: ERASING THE CUSP

C. TONINI<sup>1</sup>, A. LAPI<sup>1,2</sup>, P. SALUCCI<sup>1</sup>

*Draft version June 28, 2018*

### ABSTRACT

We propose that angular momentum transfer from the baryons to the Dark Matter (DM) during the early stages of galaxy formation can flatten the halo inner density profile and modify the halo dynamics. We compute the phase-space distribution function of DM halos, that corresponds to the density and anisotropy profiles obtained from  $N$ -body simulations in the concordance cosmology. We then describe an injection of angular momentum into the halo by modifying the distribution function, and show that the system evolves into a new equilibrium configuration; the latter features a constant central density and a tangentially-dominated anisotropy profile in the inner regions, while the structure is nearly unchanged beyond 10% of the virial radius. Then we propose a toy model to account for such a halo evolution, based on the angular momentum exchange due to dynamical friction; at the epoch of galaxy formation this is efficiently exerted by the DM onto the gas clouds spiralling down the potential well. The comparison between the angular momentum profile gained by the halo through dynamical friction and that provided by the perturbed distribution function reveals a surprising similarity, hinting at the reliability of the process.

*Subject headings:* galaxies: formation - galaxies: halos - galaxies: kinematics and dynamics - galaxies: structure - dark matter

### 1. INTRODUCTION

The Dark Matter (DM) halos produced by numerical simulations feature a cuspy density profile (Navarro et al. 1997, NFW) and a velocity distribution isotropic in the center and slightly radially anisotropic in the outer regions (Cole & Lacey 1996, Thomas et al. 1998, Huss et al. 1999).

On the other hand, recent kinematical observations in galaxies are at odds with the predicted DM distribution, favoring a cored profile (Salucci & Burkert 2000, Gentile et al. 2004). To solve this striking disagreement, several authors (*e.g.*, Spergel & Steinhardt 2000, Ahn & Shapiro 2005) recurred to a framework different from the standard cosmology (like, for instance, self-interacting DM).

We adopt an evolutionary point of view to interpret the contradiction between simulations and observations. We take for granted that a pure, unperturbed DM halo is described by a cuspy NFW profile. We recognize that the mentioned discrepancy exists precisely where the baryonic component is present (see Donato et al. 2004); this leads us to question whether the baryons themselves could be at the origin of the disagreement. Could a perturbation induced by the baryons affect the dynamics and structure of the inner halo in such a way that the original cuspy profile is modified in a corelike structure?

To test this possibility, we perform a specific study of the dynamical microscopic properties of the DM halo through the phase-space distribution function (DF), to conclude that a transfer of angular momentum is the main phenomenon at work in erasing the cusp. In fact, an angular momentum injection modifies both the orbital energy of the DM particles and the velocity distribution within the halo, breaking the symmetry of the system and leading to a completely new equilibrium configuration.

Among the physical mechanisms viable to dynamically couple the baryons to the DM we follow the approach proposed by El-Zant et al. (2001, 2004), according to which the interaction between the baryons and the halo is due to dynamical friction. The latter is exerted by the DM on the clumpy material that falls into the center of the halo during galaxy formation, and could be responsible for the halo expansion and the transformation of the profile (for complementary analysis see also Mo & Mao 2004, and Navarro et al. 1996). In this framework, we specifically focus on angular momentum transfer, and show that it can account for the halo evolution described by our treatment of the DF perturbation.

The plan of the paper is as follows: in Section 2 we compute the DF that corresponds to the density and anisotropy profiles extracted from  $N$ -body simulations; in Section 3 we perturb the DF with angular momentum and show that a new equilibrium configuration is attained, where the cusp has been smoothed out into a corelike feature and the dynamics is dominated by tangential motions; in Section 4 we present a physically-motivated toy model of angular momentum transfer between the baryons and the DM halo, based on dynamical friction; in Section (5) we summarize and discuss our findings.

### 2. THE NFW DISTRIBUTION FUNCTION

The hierarchical growth of the DM structures, as obtained from  $N$ -body simulations, produces a density profile of the virialized halos fitted by (Navarro et al. 1997)

$$\rho = \frac{M_H}{4\pi R_H^3} \frac{c^2 g(c)}{x(1+cx)^2}; \quad (1)$$

<sup>1</sup> Astrophysics Sector, SISSA/ISAS, Via Beirut 2-4, I-34014 Trieste, Italy.

<sup>2</sup> Dip. Fisica, Università "Tor Vergata", Via Ricerca Scientifica 1, I-00133 Roma, Italy.

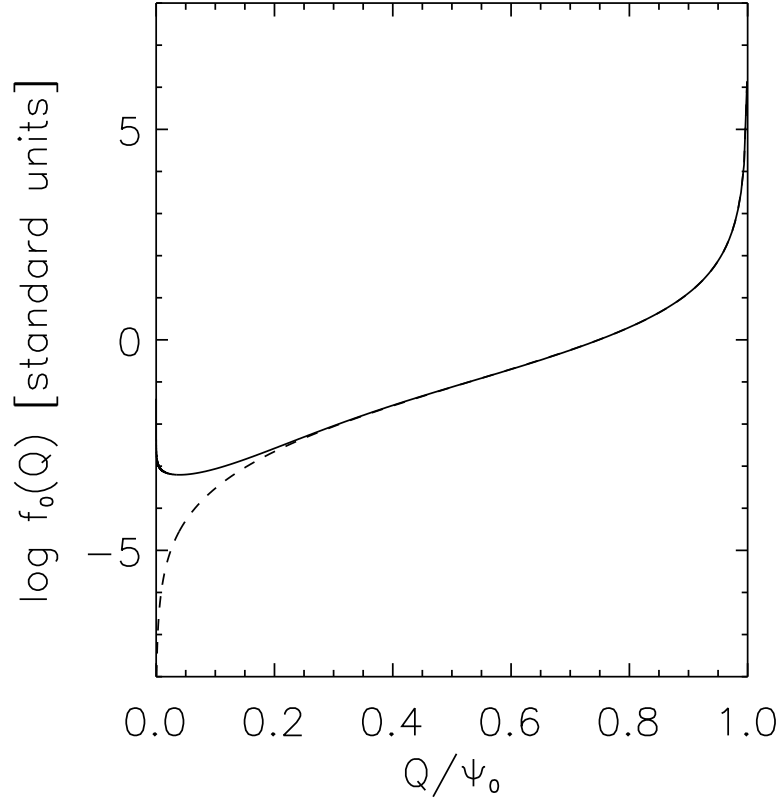


FIG. 1.— The phase-space distribution function for a NFW halo, in standard units of  $G = M_H = R_H/2 = 1$ , see Lokas & Mamon (2001). *Solid line*: halo isotropic in the center and radially anisotropic at the outskirts; *dashed line*: totally isotropic.

here  $M_H$  and  $R_H$  are the virial mass and radius,  $x = r/R_H$  is the radial coordinate,  $c$  is the concentration parameter, and  $g(c) \equiv [\ln(1+c) - c/(1+c)]^{-1}$ . The NFW gravitational potential is obtained through the Poisson equation  $\nabla^2\Phi = 4\pi G\rho$  as

$$\Phi = -V_H^2 g(c) \frac{\ln(1+cx)}{x}, \quad (2)$$

where  $V_H \equiv \sqrt{GM_H/R_H}$  is the virial velocity; hereafter, we shall express all the physical quantities in terms of  $M_H$ ,  $R_H$  and  $V_H$ .

The microscopic dynamical properties of the DM halo are linked to its macroscopic density through

$$\rho(r) = \int f(r, v) d^3v, \quad (3)$$

where  $f$  is the halo phase-space DF, which is a function of all the integrals of motions, and its symmetry properties determine those of the system. Any macroscopic observable  $O$  is obtained by means of  $f$  through the average  $\langle O \rangle = \int O f d^3v / \int f d^3v$ .

In the simple case of a totally isotropic halo,  $f$  is a function of energy alone, uniquely determined from the density profile. By conventionally defining the relative potential and binding energy as  $\Psi = -\phi$  and  $\varepsilon = -E = \Psi - \frac{1}{2}v^2$  (Łokas & Mamon 2001), the DF is obtained from the potential-density pair through the Eddington's inversion formula (see Binney & Tremaine 1987)

$$f(\varepsilon) = \frac{1}{\sqrt{8\pi^2}} \frac{d}{d\varepsilon} \int_0^\varepsilon \frac{d\rho}{d\Psi} \frac{d\Psi}{\sqrt{\varepsilon - \Psi}}. \quad (4)$$

However, the simulated halos show a nontrivial anisotropy profile; the degree of anisotropy is commonly expressed through the parameter

$$\beta(r) = 1 - \frac{\sigma_t^2}{\sigma_r^2}, \quad (5)$$

where  $\sigma_t^2$  and  $\sigma_r^2$  are the tangential and radial velocity dispersion respectively. In simulations the halos turn out to be isotropic in the center ( $\beta = 0$ ), and radially anisotropic ( $\beta > 0$ ) outwards.

For anisotropic spherical systems,  $f$  is a function of both energy and total angular momentum  $L^2$ , and there are infinite allowed DFs that satisfy Eq. (3). We focus on a DF of the form

$$f(Q, L^2) = f_0 \left( \varepsilon - \frac{L^2}{2r_a^2} \right) (L^2)^\alpha, \quad (6)$$

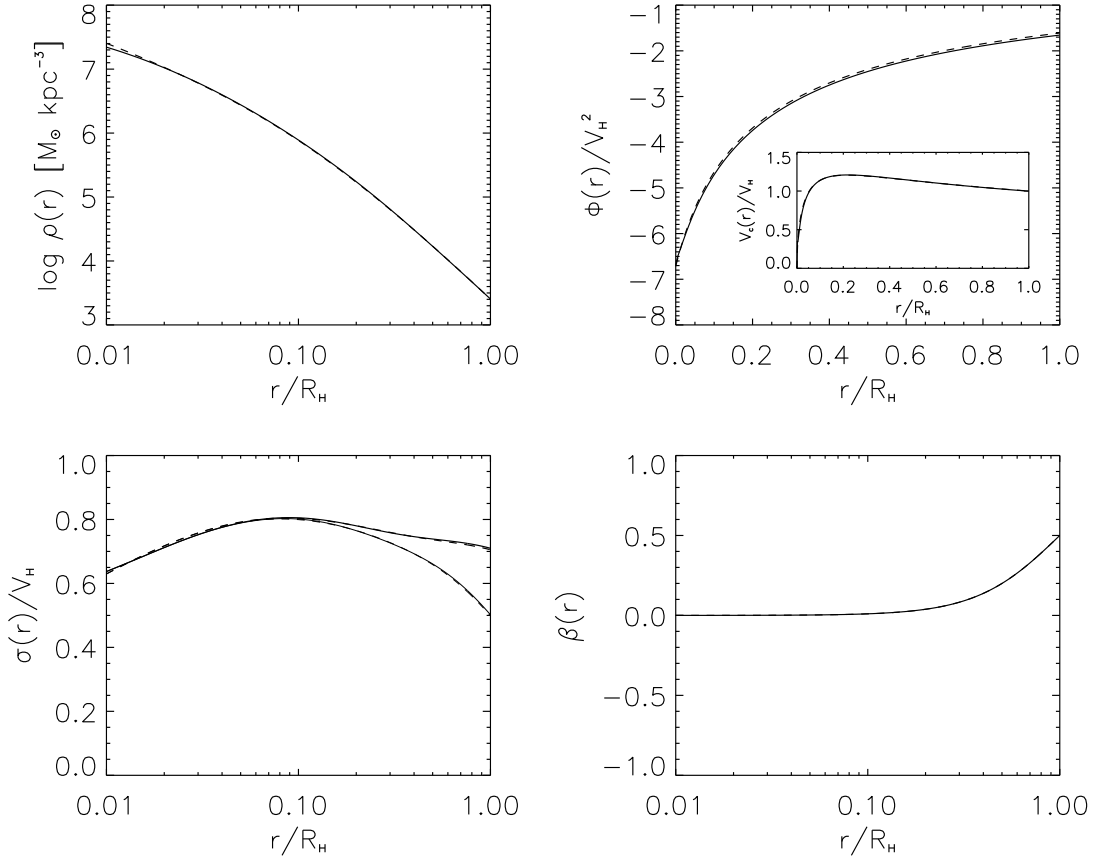


FIG. 2.— The reconstructed NFW halo (solid lines) compared to the original one (dashed lines). Upper left panel: logarithmic density profile; upper right: gravitational potential and rotation curve (inset); lower left: velocity dispersions profiles, radial (thick) and tangential (thin); lower right: anisotropy profile.

with  $r_a$  being the anisotropy radius. The angular momentum  $\vec{L}(r) = \vec{r} \times \vec{v}_T(r)$  is defined in terms of the tangential velocity  $\vec{v}_T(r)$ ; this is the 2D vectorial sum (on spheres of radius  $r$ ) of all the bulk velocities orthogonal to the radial direction, and is a measure of the tangential component of the internal, randomly-oriented motions of the halo. The orbital energy  $L^2/2r_a^2$  associated with  $L$  lowers the binding energy to give  $Q = \varepsilon - L^2/2r_a^2$  (Osipkov 1979; Merritt 1985; Binney & Tremaine 1987). In addition, the pure angular momentum component of the DF is a simple functional form, a power-law of index  $\alpha$ .

By transforming the coordinate system from  $(v_r, v_T)$  to  $(Q, L^2)$  in Eq. (3), we can express the reconstructed density profile as

$$\rho(r) = \frac{2\pi}{r^2} \int_0^\Psi f_0(Q) dQ \int_0^{2r^2(\Psi-Q)/(1+r^2/r_a^2)} \frac{(L^2)^\alpha dL^2}{\sqrt{2(\Psi-Q) - (L^2/r^2)(1+r^2/r_a^2)}} \quad (7)$$

(for details see Binney & Tremaine 1987, Chapters 4.4 - 4.5). In spherical symmetry, the averaged 1D-components of the velocity are null, and the first non-zero moments are the radial and tangential velocity dispersions

$$\sigma_r^2(r) = \frac{2\pi}{\rho r^2} \int_0^\Psi f_0(Q) dQ \int_0^{2r^2(\Psi-Q)/(1+r^2/r_a^2)} (L^2)^\alpha \sqrt{2(\Psi-Q) - \frac{L^2}{r^2} \left(1 + \frac{r^2}{r_a^2}\right)} dL^2, \quad (8)$$

$$\sigma_t^2(r) = \frac{\pi}{\rho r^4} \int_0^\Psi f_0(Q) dQ \int_0^{2r^2(\Psi-Q)/(1+r^2/r_a^2)} \frac{L^2 (L^2)^\alpha}{\sqrt{2(\Psi-Q) - (L^2/r^2)(1+r^2/r_a^2)}} dL^2, \quad (9)$$

with the total velocity dispersion being  $\sigma^2(r) = \sigma_r^2(r) + 2\sigma_t^2(r)$ ; thus the anisotropy profile reads

$$\beta(r) = \frac{r^2 - \alpha r_a^2}{r^2 + r_a^2}. \quad (10)$$

Notice that, for positive  $\alpha$ , the anisotropy is tangential in the inner regions where  $r^2 < \alpha r_a^2$ , zero at  $r^2 = \alpha r_a^2$  and radial in the outer regions where  $r^2 > \alpha r_a^2$ ; on the other hand, if  $\alpha$  is negative the model is radially anisotropic everywhere and for all values of  $r_a$ ;

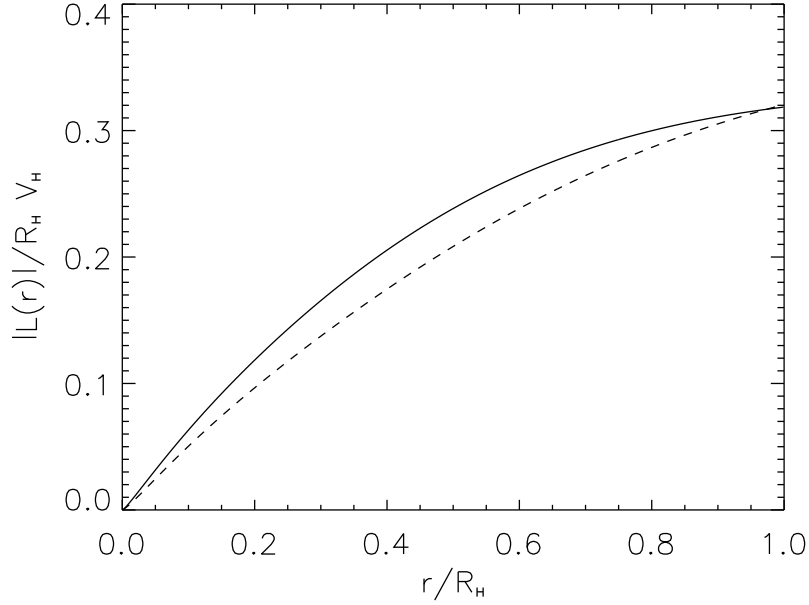


FIG. 3.— Angular momentum profile yielded by the new phase-space DF (*solid line*), compared to the unperturbed NFW one (*dashed line*), under the same unevolved gravitational potential.

therefore we conclude that, with such a DF,  $\alpha = 0$  for the NFW simulated halo. Moreover, we set the value of the anisotropy radius  $r_a \simeq 1$  (Łokas & Mamon 2001). With this choice of  $\alpha$  and  $r_a$  we obtain an isotropic inner region and a radially anisotropic outer region.

Under these conditions, the relation between the DF and the density profile reads (Cuddeford 1991)

$$f_0(Q) = \frac{1}{2^{5/2}\pi^2} \frac{d^2}{dQ^2} \int_0^Q \left(1 + \frac{r^2}{r_a^2}\right) \rho(\Psi) d\Psi. \quad (11)$$

In Fig. 1 we plot the energy part of the DF defined by Eq. (6, 11), for  $\alpha = 0$  and  $r_a \simeq 1$  (*solid line*), compared with that of a totally isotropic halo (*dashed line*).

In Fig. 2 we show the halo as reconstructed through the DF defined by Eqs. (6, 11) (*solid lines*), compared with the original NFW (*dashed lines*); in the upper panels we show the logarithmic density profile (*left*), and the gravitational potential (*right*), as well as the rotation curve (*inset*). In the lower left panel, we show the velocity dispersion profiles for the radial (*thick*) and the tangential (*thin*) components; this halo is isotropic in the inner 10% of the virial radius, and becomes radially anisotropic in the outer regions, as mirrored by the anisotropy parameter profile (*right*).

Once we know a suitable DF, we can investigate the specific angular momentum profile, that is defined as follows:

$$\langle L(r) \rangle = \frac{2\pi}{\rho r^2} \int_0^\Psi f_0(Q) dQ \int_0^{2r^2(\Psi-Q)/(1+r^2/r_a^2)} \frac{L(L^2)^\alpha}{\sqrt{2(\Psi-Q) - (L^2/r^2)(1+r^2/r_a^2)}} dL^2. \quad (12)$$

Notice that, even if the averaged 1D velocities are null, the averaged angular momentum is nonzero, due to the symmetry of the DF, as discussed after Eq. (6). This is plotted as the dashed line of Fig. 3.

### 3. PERTURBING THE HALO: THE ANGULAR MOMENTUM TRANSFER

From the above description of the halo, we can argue that the mass distribution of the system is strictly linked to its dynamics. The question that now arises is the following: is the halo stable against perturbations in its dynamical state? In other words, suppose that the halo becomes involved in a process that causes a variation in its DF function, such as an increase of energy and angular momentum; will the macroscopic observables, like the density profile, the gravitational potential and the anisotropy profile, be affected?

We defer the reader to the next section for a toy model of angular momentum transfer between baryons and DM during the first stages of galaxy formation, and we proceed now to analyze its effects on the equilibrium state of the halo.

Consider a system described by the DF of Eqs. (6, 11), and suppose to inject angular momentum into it; this translates into an increase of the particle orbital energy, that becomes  $L^2/2r_a^2 + \Delta(L^2/2r_a^2)$ , and into a variation of the power-law index  $\alpha$ . Since the DF is function of both energy and angular momentum, the halo is bound to conserve  $E$  and  $L^2$  before the perturbation, and  $E + \Delta E$  and  $L^2 + \Delta L^2$  afterwards, redistributing the excess and rearranging the DM particles in the 6D-space of coordinates and velocities. This in turn implies an evolution of the gravitational potential; hence, the system moves towards a new equilibrium configuration of density and velocity.

The process is governed by the Poisson equation

$$\frac{d^2\Psi}{dr^2} + \frac{2}{r} \frac{d\Psi}{dr} = 4\pi G \int_0^\Psi \int_0^{2r^2(\Psi-Q)/(1+r^2/r_a^2)} f(Q, L^2) dL^2 dQ \quad (13)$$

where  $\alpha$  and  $r_a$  are now to be intended as the new, perturbed parameters. This integro-differential equation has to be solved for  $\Psi$ ; the resulting potential, density and anisotropy profiles are the observables of the new equilibrium state of the halo. While the complete integration has to be done iteratively, the solution for small radii is analytical, and gives an interesting insight on the behavior of the halo.

Before proceeding, note that the density profile of Eq. (7) can be written as

$$\rho(r) = \frac{(2\pi)^{3/2} 2^\alpha r^{2\alpha}}{(1+r^2/r_a^2)^{\alpha+1}} \frac{\Gamma(\alpha+1)}{\Gamma(\alpha+3/2)} \int_0^\Psi f_0(Q)(\Psi-Q)^{\alpha+1/2} dQ, \quad (14)$$

after the integration in  $L^2$  is performed explicitly. For small radii, *i.e.* when  $Q \rightarrow \varepsilon \rightarrow \Psi_0$ , with  $\Psi_0$  the central value of the potential, it is easy to see that  $\rho(r) \propto 1/r \propto 1/[\Psi_0 - \Psi(r)]$ ; by changing variable in Eq. (11) from  $\varepsilon$  to  $(\varepsilon - \Psi)/(\Psi_0 - \varepsilon)$ , the energy part of the DF behaves like

$$f_0(\varepsilon) \propto (\Psi_0 - \varepsilon)^{-5/2}. \quad (15)$$

Putting this expression into Eq. (14), and passing from  $\varepsilon$  to  $(\Psi - \varepsilon)/(\Psi_0 - \Psi)$ , the density profile at small radii is found to behave as

$$\rho(r) \propto [\Psi_0 - \Psi(r)]^{\alpha-1} r^{2\alpha}. \quad (16)$$

This expression is now inserted into the Poisson equation (13), to obtain the self-consistent solution for the new potential  $\Psi(r)$ , which reads

$$\Psi_0 - \Psi(r) \propto r^{2(\alpha+1)/(2-\alpha)}. \quad (17)$$

Finally, the new density profile  $\rho(r)$  from Eq. (16) reads

$$\rho(r) \propto r^{-2(1-2\alpha)/(2-\alpha)}; \quad (18)$$

thus we find that for  $\alpha \rightarrow 0$  the inner profile behaves like  $r^{-1}$  (NFW), while for  $\alpha \rightarrow 1/2$  we obtain  $\rho(r) \rightarrow \text{constant}$ .

In addition, the anisotropy parameter defined by Eq. (10) behaves like  $\beta(r) \rightarrow -\alpha$ , and for  $\alpha = 1/2$  the halo features a constant tangential anisotropy in the inner regions. The inner specific angular momentum profile depends on the value of  $\alpha$  as well, and is obtained as

$$L(r) \propto r [\Psi_0 - \Psi(r)]^{1/2} \propto r^{3/(2-\alpha)}; \quad (19)$$

for the unperturbed halo  $L(r) \rightarrow r^{3/2}$  and for  $\alpha = 1/2$  we get  $L(r) \rightarrow r^2$ .

Beside these analytical results, we performed the full numerical integration of Eq. (13). As a boundary condition throughout this computation we adopted the halo mass conservation; we further normalized the evolved potential in order to obtain the same behavior of the outer rotation curve as before.

It is interesting to analyze this process in two steps: since the density and anisotropy profiles and the potential well evolve together, it is impossible to evaluate the variation in the angular momentum of the system after the new equilibrium state is reached, because the system has then lost memory of its initial conditions. Instead, suppose to picture the halo at the moment when the DF received its input in energy and angular momentum, but the potential well has not yet evolved; then we can evaluate the amount of angular momentum that has been injected into the halo. In Fig. 3 we show the specific averaged angular momentum profiles as yielded by the old, NFW-like (*dashed*), and new (*solid*) DFs, in the same potential. Keep in mind that this is not a stable state, the system is going to evolve into a configuration that satisfies the Poisson equation.

The final configuration of the system, corresponding to its new equilibrium state, is showed in Fig. 4. The density profile (*upper left*) has been smoothed and the cusp erased; this mirrors the mass loss by the inner regions of the halo, since the DM particles have been moved to more energetic orbits. Notice the corresponding flattening of the potential well (*upper right*). Accordingly, the rotation curve (*inset*) is more gently rising in the inner regions and is nearly unchanged beyond half of the virial radius.

As to the velocity dispersion, the symmetry between the radial and tangential motions has been broken in favor of the latter (*lower left*); relatedly, the anisotropy parameter profile (*lower right*) is now negative in the inner halo and changes sign at a radius corresponding to the new  $r_a = 1/\sqrt{2}$ , that is set by requiring the same outermost value of  $\beta(r)$  as before, although it scarcely affects the results shown above.

In sum, given the DF of equation (6), the couple ( $\alpha = 0$ ,  $r_a \sim 1$ ) describes the known NFW halo, cuspy and almost entirely isotropic, while the couple ( $\alpha = 1/2$ ,  $r_a \sim 1/\sqrt{2}$ ) produces a corelike halo, with a constant inner density profile and a tangentially-dominated inner anisotropy profile.

We point out that the injection of angular momentum corresponding to our DF produces additional bulk rotational motions, though they are not to be intended as *ordinate* in the common sense of the word; in fact, the symmetry of the halo and its dynamics are defined by that of the DF, and therefore there is not a definite preferential direction of rotation. The DM particles move on orbits around the center of mass with random orientations, so that the resulting angular momentum  $L^2$  is nonzero, but the average value of each velocity component is null.

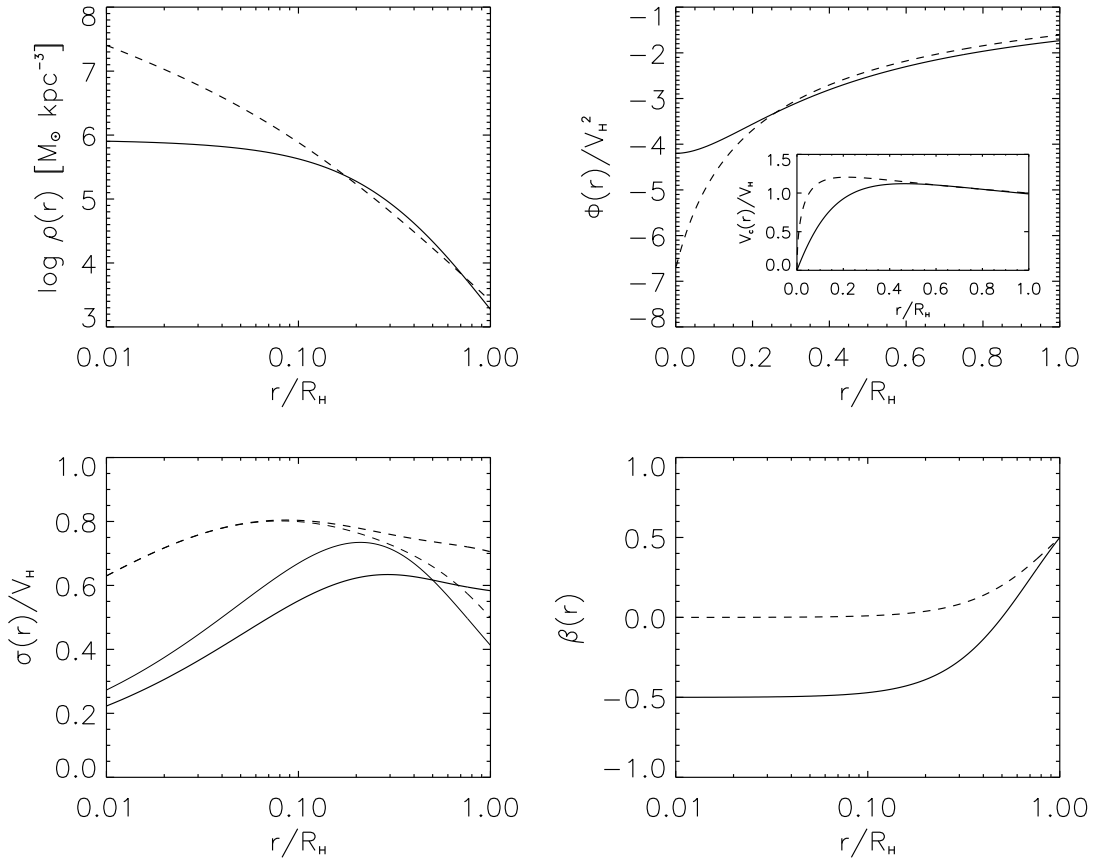


FIG. 4.— New equilibrium configuration of the perturbed halo (*solid lines*), compared to the NFW (*dashed lines*). *Upper left panel:* logarithmic density profile; *upper right:* gravitational potential and rotation curve (*inset*); *lower left:* velocity dispersions profiles, radial (*thick*) and tangential (*thin*); *lower right:* anisotropy profile.

#### 4. DYNAMICAL FRICTION AS AN ANGULAR MOMENTUM ENGINE

Now the issue arises: Is there a physical process that can account for the evolution described above? In this section we aim at presenting a toy model that provides the halo with such an amount of angular momentum to allow its DF to evolve from a cuspy to a cored configuration. The natural framework is galaxy formation, when the baryons collapse inside the dark halo potential well and exchange angular momentum with the DM through dynamical friction.

Specifically, in the very early stages of galaxy formation, the baryons trapped inside the potential wells of the halos undergo radiative dissipation processes that cause them to lose kinetic energy and to form clumps inside the relatively smooth dark halo. If radiative cooling is effective, the gas will organize into self-gravitating clouds before it collapses to the halo center and condenses into stars; the clouds are likely to survive the tidal stripping due to the DM, because of their relatively high binding energy (Mo & Mao 2004). The clumpy gas component decouples from virial equilibrium, and dissipates its orbital energy; in detail, the clouds spiralling down get closer and closer to the halo center, increasing their tangential velocity along their orbits and reaching regions with higher and higher density.

In these regions, a gravitational effect becomes relatively efficient in slowing down the clouds, namely the dynamical friction exerted by the background DM particles, that causes part of the cloud velocity to be transferred from the baryons to the DM itself (El-Zant et al., 2001, 2004). As a result, the inner part of the halo is granted with a surplus of angular momentum and energy, depending on the number, mass and initial velocity of the clouds.

Consider a cloud of mass  $M_c$  that at time  $t = 0$  is at a certain distance from the center of the halo, with initial velocity  $v^2 = v_r^2 + (L/r)^2$  and angular momentum  $L$ ; we define the initial pericenter of its orbit as  $r_+(0)$ , the eccentricity as  $e(0)$ , and the apocenter as  $r_-(0) = r_+(1 - e)/(1 + e)$ . The cloud is self-gravitating and hence we consider it as a point mass, immersed in the halo potential well; in the orbit-averaged approximation (Lacey & Cole 1993), the equations of motions for the cloud energy and angular momentum are given by

$$\frac{dE}{dt} = - \frac{\int_{r_-}^{r_+} (1/v_r) v |F_{\text{fric}}| / M_c dr}{\int_{r_-}^{r_+} (1/v_r) dr}, \quad (20)$$

TABLE 1  
DYNAMICAL FRICTION RESULTS

$\delta^a$	$\langle N_i \rangle^b$	$\langle M_c \rangle^c$	$\langle \Delta L_{DM} \rangle^d$	$M_g$ (2 Gyr) <sup>e</sup>	$M_g$ (6 Gyr) <sup>f</sup>
0	31.45	5.03e-3	1.04	0.039	0.074
1	109.66	1.46e-3	1.86	0.032	0.064
2	2276.98	7.05e-5	7.54	0.019	0.043

NOTE. — Column label: (a) cloud power-law mass function index; (b) average number of clouds; (c) average cloud mass (units of  $M_H$ ); (d) average of the exchanged specific angular momentum (units of  $R_H V_H$ ) integrated over the profile; (e) average baryonic mass that falls inside  $0.1 R_H$  after 2 Gyr and, (f) after 6 Gyr (units of  $M_H$ ).

$$\frac{dL}{dt} = - \frac{\int_{r_-}^{r_+} (1/v_r) L |F_{\text{fric}}| / (M_c v) dr}{\int_{r_-}^{r_+} (1/v_r) dr}, \quad (21)$$

with initial conditions set by

$$L(0) = \sqrt{\frac{2[\Psi(r_+) - \Psi(r_-)]}{1/r_+^2 - 1/r_-^2}}, \quad E(0) = \Psi(r_+) + \frac{v^2(r_+)}{2}. \quad (22)$$

At each instant, the force exerted by the background DM particles on the cloud is

$$|F_{\text{fric}}| = -4\pi G^2 M_c^2 \ln \Lambda \frac{\int_0^v f(v') d^3v'}{v^2}, \quad (23)$$

in terms of the NFW phase-space distribution function  $f$  (see Section 2), of the cloud speed  $v = \sqrt{2[\Psi(r) - E(t)]}$  and of the Coulomb logarithm  $\ln \Lambda = \ln(M_H/M_c)$ . At each timestep,  $r_{\pm}(t)$  are given by the condition  $v_{\mp}^2 = \sqrt{v^2 - L^2/r^2} = 0$ . Due to the dynamical friction, the orbit shape and the velocity of the cloud evolve in time, so that this set of equations has to be solved iteratively.

For a halo of virial mass  $M_H$  we performed a series of Montecarlo simulations for different ensembles of clouds, characterized by a mass function scaling as  $M_c^{-\delta}$ , with index  $\delta$  ranging from 0 to 2; in each realization, we allowed the cloud masses to range from  $10^{-5}$  to  $10^{-2} M_H$  (El-Zant et al. 2004). The number of clouds is actually constrained by the total amount of baryons, set to equal the cosmological fraction  $0.16 M_H$ . The initial spatial distribution of the clouds is uniform between  $r = 0$  and  $r = R_H$ ; at time  $t = 0$  the clouds are in statistical equilibrium with the background halo, therefore their initial velocities are randomly sampled from a Maxwellian distribution, with mean 0 and variance  $\langle \sigma_{t,r}^2 \rangle / 2$ .

For each  $\delta$  we performed 100 runs, and computed the average specific angular momentum transferred by the clouds to the halo after 2 Gyr; we expect that after this time the inner part of the halo becomes so crowded with clouds that they start to collide and disrupt, and the star formation effects dominates over the dynamics of the gas (El-Zant et al. 2004). However, in the outer regions the process continues with longer timescales, so that we also followed the evolution of the system for about 6 Gyr.

In Table 1, for each  $\delta$  we give the average number and mass of the clouds, the total angular momentum gained by the halo, and the mass accumulated in the center of the halo after 2 and 6 Gyr. Note that with our power-law mass functions, the massive clouds constitute a small fraction of the total; on the other hand, the dynamical friction is more effective on them, and therefore they have a large probability to lose all their angular momentum quickly, and to collapse in the center of the halo soon. The small clouds instead take more time to spiral down in the halo potential well, and retain a larger fraction of their initial angular momentum. In the end, a steeper mass function, that selects a high number of small clouds, results in a more effective transfer of angular momentum to the halo.

In Fig. 5 we illustrate an example of the time evolution of a set of clouds sampled with power-law index  $\delta = 1$ . In the time interval from  $t = 0$  to  $t = 6$  Gyr a fraction of the clouds reaches the inner 10% of the virial radius (upper panel), building up the mass that is likely to end up in the spheroidal component of the forming galaxy. In the middle panel we show the evolution of the orbit eccentricity, and in the lower panel the angular momentum lost by the single clouds and transferred to the halo. Notice that the fraction of clouds that effectively transfer angular momentum to the halo is relatively small, and that the majority of the clouds remains on almost unperturbed high orbits, meaning that the timescales of dynamical friction are long. This effect is enhanced for increasing  $\delta$ , as shown in the last two columns of Table 1; a steeper mass function results in a slower accumulation of baryons in the center. In any case, the final amount of baryons inside the inner 10% of the virial radius after 2 and 6 Gyr is overabundant with respect to the known galactic masses (spheroidal and/or disk components; see Shankar et al. 2006), due to the fact that the total baryonic component initially matches the cosmological fraction. However, while baryons accumulate in the center of the potential well and organize themselves into the protogalactic structure, star formation and AGN activity start, along with the ensuing feedback processes that eventually regulate the actual amount of baryons.

Notice that these feedback mechanisms can in no way affect the transfer of angular momentum between the visible and dark components, as they take place after the cloud collapse; as will be discussed in the next section, the growing baryonic mass at the center of the halo could affect the final dynamical state of the system only marginally.

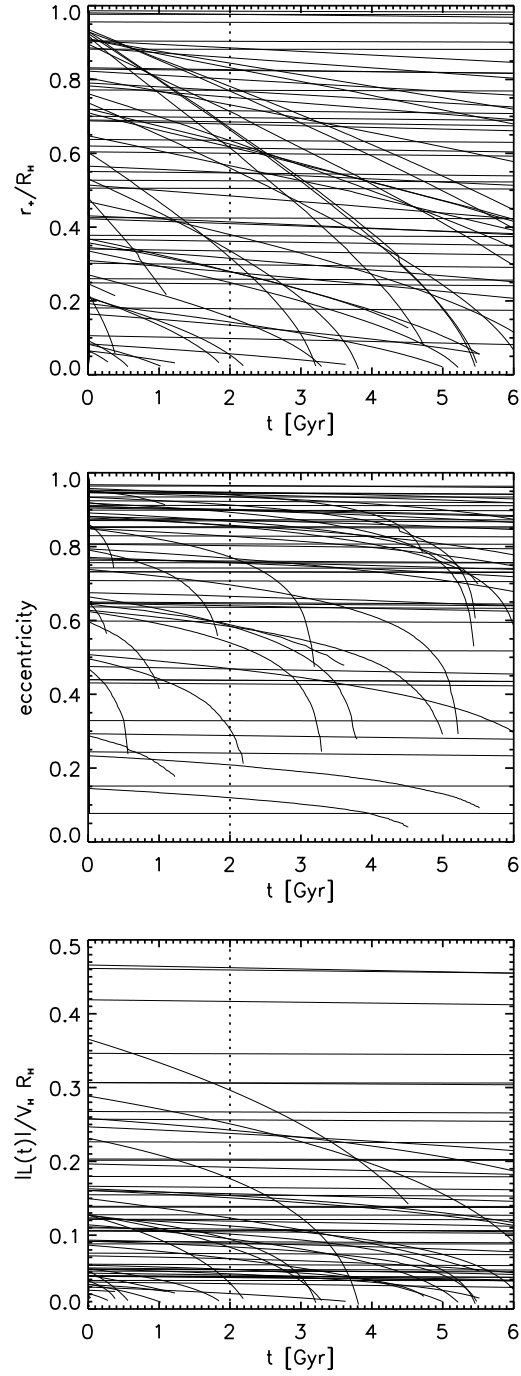


FIG. 5.— Time evolution of a set of clouds sampled with power-law index  $\delta = 1$ . *Upper panel*: apocenter of the orbit; *middle panel*: orbit eccentricity; *bottom panel*: angular momentum retained by the clouds.

In Fig. 6 we present the final angular momentum profile of the halo, for  $\delta = 0, 1, 2$ . From each run of our simulation we extract a transferred momentum profile after 2 Gyr and then add it to the original NFW (*dashed lines*, see also Fig. 3); the *shaded areas* represents the overlap of all the resulting new profiles. For comparison, we plot the profile obtained in Section 3 through the transformation of the DF (*solid lines*, see also Fig. 3).

The angular momentum profile produced through the dynamical friction mechanism is clearly compatible with that resulting from the perturbation of the halo DF described in Section 3. In fact, the effect of the dynamical friction on the halo is that of enhancing the tangential motions with respect to the radial; this is the same behavior expected in a halo whose DF is a function of  $L^2$ , regardless of the details in the shape of the DF itself.



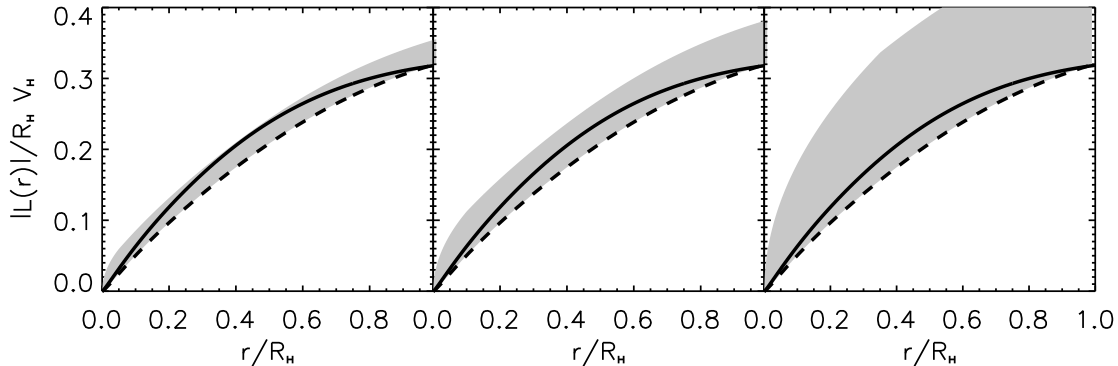


FIG. 6.— Comparison between the angular momentum profiles implied by the phase-space DFs and by dynamical friction. *Dashed line*: unperturbed NFW halo (see Section 2); *solid line*: perturbed halo, new DF (see Section 3); *shaded regions*: NFW angular momentum profile plus  $\Delta L$  from dynamical friction, for  $\delta = 0$  (left),  $\delta = 1$  (center) and  $\delta = 2$  (right).

## 5. DISCUSSION AND CONCLUSIONS

We approached the topic of the coevolution of the baryons and their host DM halo, to investigate whether the mechanism of galaxy formation can flatten the inner halo density profile and reconcile the observational evidences with the standard theory of hierarchical clustering.

We performed two independent computations over the NFW halo, one perturbing its phase-space distribution function with angular momentum, the other following the evolution of the baryonic angular momentum during the collapse inside the halo potential well; we are faced with the conclusion that both of them are viable to describe the halo evolution due to galaxy formation, the former from the microscopic and the latter from the macroscopic point of view.

We showed, through the study of the microscopic dynamical properties of the DM, that the NFW halo is strongly sensitive to angular momentum transfer; an injection of angular momentum to the DM produces a flattening of the density profile and a redistribution of the particles in velocity space, with an increase of the fraction of tangential motions over the total velocity dispersion.

From the macroscopic side, we looked for a mechanism of angular momentum transfer that directly involved the baryons, that was especially efficient during galaxy formation, and that directly affected the microscopic state of the system; thus we focused on dynamical friction (El-Zant et al., 2001, 2004). Notice that such a process is well below the current resolution limit of the cosmological numerical simulations; however, it is implemented in recent simulations of cluster and galactic size halos (Nipoti et al. 2004, Ma & Boylan-Kolchin 2004). In fact, angular momentum can be transferred also by tidal interactions and mergers; however, such events are less and less frequent with decreasing redshift both for spheroidal galaxies (Koopmans et al. 2006, Dominguez-Tenreiro et al. 2006) and for spirals (D’Onghia & Burkert 2004, Tonini et al. 2006). Moreover, such interactions between the halo and its neighbours occur on scales comparable to that of the halo itself, thus giving rise to global perturbations of its dynamical state and global ordinate motions; for this reason, it is more likely that such events affect the halo spin rather than the halo inner angular momentum and anisotropy profiles.

When modeling the phase-space DF, we had to face the degeneracy intrinsic to this kind of problem, that allows infinite functions to satisfy the Poisson equation. The symmetry of the system is set by that of the DF; for an isotropic system, the only integral of motion is energy, and  $f$  is uniquely determined. But if the symmetry between the radial and tangential velocity components is broken, then  $f$  becomes  $f(\varepsilon, L^2)$ ; the system is bound to conserve the internal angular momentum, and when perturbed with a  $\Delta L^2$ , it is enforced to find a new equilibrium configuration. This is the case we considered in Section 3; we focused on a power-law in  $L^2$  due to its simplicity, and showed that it can account for the basic observables of the halo, such as the density and anisotropy profiles, and the shape of the potential. Note that this kind of DF cannot account for the halo spin, that is found to be  $\lambda \sim 0.03 - 0.06$  from simulations and observations (see Tonini et al. 2006 and references therein). This value of  $\lambda$  is small, nonetheless it gives us information on the true shape of the halo in phase-space. In fact, more generally, the system would be described by a DF of the form  $f(\varepsilon, L^2, L_z)$ , where also the symmetry between the two tangential velocity components is broken. A complete shape of the perturbed DF could be of the kind  $f(Q, L^2, L_z) = f_0(Q) f_1(L^2, L_z)$ , where  $f_1$  may be a power-law or a more complex function, odd in  $L_z$  to have net bulk rotation around the symmetry axis. With this DF the tangential velocity  $\vec{v}_T$  is parallel to the equatorial plane and the halo features a macroscopic total angular momentum in the  $z$ -direction,  $\vec{L}_z = \vec{r} \times \vec{v}_T$ , that is aligned with the spin,  $\lambda \simeq v_T / \sigma$ .

In the computation of the perturbed gravitational potential we did not include the baryonic mass, although it does have an effect on the total gravitational potential, since the baryons piling up in the center of the halo tend to deepen the well. But three considerations are needed here: 1) the right amount of baryons that is actually observed in the center of halos is deeply connected with feedback processes, that are responsible for removing at least half of the initial baryonic mass (Shankar et al. 2006); 2) as hinted in Section 1, the feedback processes themselves can transfer energy to the DM and contribute to smoothen the cusp; 3) the dominant effect in changing the equilibrium configuration of the halo is the DF symmetry breaking induced by the angular momentum transfer, while the deepening of the potential well simply produces an isotropic enhancement of all the  $\sigma$  components, that does not interfere with the described process. So, even taking into account the deepening of the total potential well due to

baryons, the effect turns out to be quite negligible.

Up to now, there is no definite knowledge of the details of the baryon collapse into the protogalactic structure. Nevertheless, if dynamical friction indeed plays a major role in the collapse, it could affect the morphology of the galaxy that is to form, possibly through its timescale that in turn depends on the cloud mass function. While massive clouds, collapsing early and losing all their momentum, can feed up the spheroidal component, the small clouds are most likely to end up in a rotating disk; in particular, the slow, gradual accretion of small clouds can be assimilated to the infall of material that causes the *inside-out* formation of disks (Chiappini et al. 1997). As a possible evidence of this process, we can consider the molecular clouds that today travel across the Galactic disk, trapped inside the potential well of the DM halo; these are too small to have actively participated in the growth of the disk, because only marginally affected by dynamical friction.

The main results of the paper are the following:

- we computed the NFW phase-space distribution function, and analyzed the internal halo dynamics, with particular focus on the anisotropy and the angular momentum profiles.
- we perturbed the NFW halo by injecting angular momentum into it, *i.e.* breaking the symmetry of its DF that becomes explicitly a function of the two variables  $E$ ,  $L^2$ ; physically speaking, the DM particles gain orbital energy and bulk tangential motions. As a consequence, the halo evolves into a new equilibrium configuration, characterized by a cored density profile, a tangential anisotropy in the inner regions, and a shallower potential well; we also computed the new angular momentum profile.
- we tested that dynamical friction exerted by the DM on the baryons at the time of protogalaxy formation is a viable mechanism to perturb the halo structure, a result in agreement with El-Zant et al. (2001, 2004). In particular we show that the transfer of angular momentum from the baryons to the DM due to dynamical friction produces an angular momentum profile consistent with the one of a halo that has been perturbed and eventually features a tangential velocity anisotropy and a corelike profile.

We consider this evolutionary approach most promising in solving the cusp-core controversy that affects the interpretation of the observational data, and in moving towards the understanding of the mechanisms of galaxy formation.

We thank the referee for her/his comments and suggestions. Work supported by grants from ASI, INAF and MIUR.

#### REFERENCES

- Ahn, K. & Shapiro, P.R. 2005, MNRAS, 363, 1092  
 An, J.H. & Evans, N.W. 2006, AJ, 131, 782  
 Binney, J. & Tremaine, S., *Galactic dynamics* (1987 Princeton: Princeton University Press)  
 Cardone, V.F., Piedipalumbo, E. & Tortora C. 2005, MNRAS, 358, 1325  
 Chiappini, C., Matteucci, F. & Gratton, R. 1997, ApJ, 477, 765  
 Cole, S. & Lacey, C. 1996, MNRAS, 281, 716  
 Cuddeford, P. 1991, MNRAS, 253, 414  
 D’Onghia, E. & Burkert, A.M. 2004, ApJ, 612, L13  
 Dominguez-Tenreiro, R., Oñorbe, J., Saiz, A., Artal, H. & Serna, A. 2006, astro-ph/0511556  
 Donato, F., Gentile, G. & Salucci, P. 2004, MNRAS, 353, L17  
 El-Zant, A., Shlosman, I. & Hoffman, Y. 2001, ApJ, 560, 636  
 El-Zant, A., Hoffman, Y., Primack, J., Combes, F. & Shlosman, I. 2004, ApJ, 607, L75  
 Evans, N.W. & An, J.H. 2005, A&A, 444, 45  
 Gentile, G., Salucci, P., Klein, U., Vergani, D. & Kalberla, P. 2004, MNRAS, 351, 903  
 Huss, A., Jain, B. & Steinmetz, M. 1999, ApJ, 517, 64  
 Kent, S.M. & Gunn, J.E. 1982, AJ, 87, 945  
 Koopmans, L.V.E., Treu, T., Bolton, A.S., Burles, S. & Moustakas, L.A. 2006, ApJ, submitted [preprint astro-ph/0601628]  
 Lacey, C. & Cole, S. 1993, MNRAS, 262, 627  
 Lokas, E.L. & Mamon, G.A. 2001, MNRAS, 321, 155  
 Louis, P.D. 1993, MNRAS, 261, 283  
 Ma C.-P. & Boylan-Kolchin M. 2004, PhRvL 93b 1301M  
 Merritt, D. 1985, AJ, 90, 6  
 Mo, H.J. & Mao, S. 2004, MNRAS, 353, 829  
 Navarro, J.F., Eke, V.R. & Frenk, C.S. 1996, MNRAS, 283, L72  
 Navarro, J.F., Frenk, C.S. & White, S.D.M. 1997, ApJ, 490, 493  
 Nipoti, C., Treu, T., Ciotti, L. & Stiavelli, M. 2004, MNRAS 355, 1119-1124  
 Osipkov, L.P. 1979, Soviet Astron. Lett., 5, 42  
 Peñarrubia, J., Just, A. & Kroupa, P. 2004, MNRAS, 349, 747  
 Salucci, P. & Burkert, A. 2000, ApJ, 537, L9  
 Shankar, F., Lapi, A., Salucci, P., De Zotti, G. & Danese, L. 2006, ApJ, in press [preprint astro-ph/0601577]  
 Spergel, D.N. & Steinhardt, P.J. 2000, Phys. Rev. Lett., 84, 3760  
 Thomas, P.A. et al. 1998, MNRAS, 296, 1061  
 Tonini, C., Lapi, A., Shankar, F. & Salucci, P. 2006, ApJ, 638, L13  
 van den Bosch, F.C., Lewis, G.F., Lake, G. & Stadel, J. 1999, ApJ, 515, 50  
 Widrow, L.M. 2000, ApJSS, 131, 39